Proc. Natl. Acad. Sci. USA
Vol. 82, pp. 755–759, February 1985
Biophysics

Molecular dynamics simulations of d(C-G-C-G-A)·d(T-C-G-C-G) with and without "hydrated" counterions

(DNA/molecular mechanics/conformational analysis/electrostatic effects)

U. C. SINGH, SCOTT J. WEINER, AND PETER KOLLMAN*

Department of Pharmaceutical Chemistry, University of California, San Francisco, CA 94143

Communicated by Robert G. Parr, August 15, 1984

ABSTRACT **We present the results of molecular dynamics simulations on d(C-G-C-G-A)·d(T-C-G-C-G) with fully charged phosphates with and without inclusion of counterions. The average structures found in the two simulations are similar, but the simulation with counterions does give an average helix repeat, tilt, and twist in better agreement with those found in the x-ray structure of d(C-G-C-G-A-A-T-T-C-G-C-G)$_2$. The average sugar pucker phases and amplitudes are in qualitative agreement with those found in NMR studies of double-helical DNA, and a number of examples of sugar repuckering from C2′ *endo* to C3′ *endo* carbon conformations in the sugar ring are found. The hydrogen bond correlations as well as torsion correlations are analyzed, and some interesting long-range correlations between dihedral angles are found.**

Molecular dynamics simulations have been shown to give interesting insights into the nature of protein and peptide flexibility (1), water structure (2), and solvation of small molecules in water (3). Fewer applications of dynamics have been made to nucleic acids than to proteins. However, recently there have been three studies of nucleic acids with molecular dynamics that have begun to remedy this deficiency. Prabhakaran *et al.* (4, 5) have studied transfer RNA and have found that the overall shape and exposed surface area of this molecule remains near the x-ray-determined one for 32 ps of simulation. Tidor *et al.* (6) have carried out harmonic normal mode analysis and 60 ps of molecular dynamics on base-paired deoxyhexanucleoside pentaphosphate d(C-G-C-G-C-G)$_2$. The magnitude of the motions found for base, sugar, and phosphate show general accord with x-ray results. Finally, Levitt (7) has carried out the most extensive study of DNA dynamics, with 90-ps simulations on d(C-G-C-G-A-A-T-T-C-G-C-G)$_2$ and dA_{24}·dT_{24}. Levitt characterized fluctuations in hydrogen bonds, torsional angles, and their correlated motions; analyzed the overall bending and twisting of these large helices; and found an example of a "kinked" double helix in the dA_{24}·dT_{24} simulation. The significant torsional correlations found were, encouragingly, those also found in the analyses of the x-ray structure of d(C-G-C-G-A-A-T-T-C-G-C-G)$_2$ (8).

The two previous studies of DNA dynamics, those of Tidor *et al.* (6) and Levitt (7), suggest that one can obtain interesting and useful results via molecular dynamics simulations of DNA. However, the two approaches differ substantially in computational detail, with Levitt omitting electrostatic partial charges from his model and Tidor *et al.* including partial changes but reducing the anionic phosphate charge from −1 to −0.2 and using a distance-dependent dielectric constant. When Levitt carried out simulations with electrostatic charges and a dielectric constant of 1.0, the DNA unwound within 50 ps. The two studies took different approaches to circumventing the fact that DNA exists in the presence of counterions and water, but their full inclusion would make the molecular dynamics simulation, in general, 1 or 2 orders of magnitude more time-consuming.

Below we present molecular dynamics simulations of the base-paired pentanucleoside phosphate d(C-G-C-G-A)·d(T-C-G-C-G) using fully anionic phosphates with and without large "hydrated" Na^+ counterions. Our goals are 3-fold: to characterize the hydrogen bonding, sugar puckers, torsional angles, helix parameters, and overall motion as a function of base; to analyze the effect of counterions on the DNA structure and dynamics; and to "set the stage" for parallel studies of mismatched base pair analogs of the above sequence and for dynamics studies of the same sequence with counterions and water using a dielectric constant $\varepsilon = 1$.

METHODS

Two molecular dynamics simulations used the program AMBER (9) and were carried out on d(C-G-C-G-A)·d(T-C-G-C-G), one with and one without large "hydrated" counterions. We evaluated the energy and forces of the system using the molecular mechanical parameters reported by Weiner *et al.* (10) with a distance-dependent dielectric model, $\varepsilon = R_{ij}$. The only additional parameters required were the nonbonded terms to represent the cation, where we used a charge of +1.0, a van der Waals radius $R = 5.0$ Å, a well depth of $\varepsilon =$ 0.1 kcal/mol (1 cal = 4.184 J), and a mass of 131 atomic mass units corresponding to hexahydrated Na^+. This large radius was designed to mimic the effect of aqueous hydration of Na^+ and phosphate anion and to keep "contact" ion pairs from forming.

We started with the B-DNA geometry of Arnott *et al.* (11) and energy-refined it for 500 cycles with conjugate gradient minimization. In the simulation with counterions, the counterion was initially placed along the PO_2^- bisector and 6 Å from the phosphorus, but no restraint was placed on any atoms during the simulation.

The simulations were begun by assigning random velocities that followed a Maxwellian distribution at 298 K to the atoms and then equilibrating the system for 3 ps by using a temperature-coupling parameter of 0.5 ps^{-1} (12). A further equilibration of the system for 9 ps used a coupling parameter of 0.2 ps^{-1}. The simulations were then continued with 0.2 ps^{-1} temperature coupling for 83 ps, and the results reported are averages over this time period. The time step of the dynamics was 0.001 ps, and a Verlet "leap-frog" integrator algorithm (12) was used to solve the equations of motion by numerical integration. The temperature during the simulation fluctuated around 298 K by ±10 K, and the change in the total energy was <0.02 kcal/mol for each time step.

The first 12 ps of the run without counterions was carried out without a nonbonded cutoff and with a nonbonded cutoff of 12 Å. The similarity of the results of the two simulations

The publication costs of this article were defrayed in part by page charge payment. This article must therefore be hereby marked "*advertisement*" in accordance with 18 U.S.C. §1734 solely to indicate this fact.

*To whom reprint requests should be addressed.

led us to continue the remaining calculations with a 12-Å cutoff, with the nonbonded list updated every 0.2 ps.

AVERAGE STRUCTURAL PARAMETERS

Table 1 contains the average dihedral angle values for 83 ps of simulations of d(C-G-C-G-A)·d(T-C-G-C-G) with and without counterions. An analysis of the first 45 ps of dynamics of the molecule with counterions led to similar average dihedral angles as the average over 83 ps, so we report only the full 83-ps average. As one can see, the average dihedral angles from the two simulations are within the standard deviations of each other, particularly when the terminal base pairs, which undergo conformational transitions, are removed from the average.

A detailed examination of the individual dihedral angle averages and a visualization of the dynamics trajectory revealed significantly larger distortions in the end base pairs (see below) in the simulation without counterions. Much of this greater distortion could be attributed to the fact that, during the simulation without counterions, the 5′ OH groups on both strands moved to form hydrogen bonds with the nearest phosphate on each strand. Such hydrogen bonds did not form in the simulation with counterions.

In both simulations, there were a number of "conformational transitions" during the dynamics, involving mainly those dihedral angles near the end of the chain. In Fig. 1 we present for the simulation with counterions the time course of the thymine ψ' (sugar pucker), which stays near the C2′ *endo* conformation throughout the first 55 ps of the simulation and then undergoes a rapid conversion to the C3′ *endo* conformation.

The standard deviations of each of the dihedral angles also give insight into the inherent flexibility of each angle, since the averages are not only over different angles but also, for each angle, are over all the time steps (in measurements of 0.1 ps). By factoring out those terminal base pairs that have undergone conformational transitions, ω' is the most "flexible" of the five backbone single-bond dihedral angles, and ψ is the least flexible (independent of simulation model). The other three such angles, ϕ', ϕ, and ω, are intermediate. These results are in qualitative agreement with molecular mechanics calculations on longer sequences (13) and with standard deviations in the x-ray structure (8) of d(C-G-C-G-A-A-T-T-C-G-C-G)$_2$.

The angle involving the sugar ring, ψ', and the glycosidic angle χ for the pyrimidine bases differ most between the two simulations, but their respective standard deviations still overlap.

Table 1. Average dihedral angles*

Angle	With counterions	Without counterions
ψ	58.5 ± 9.2 (58.1 ± 8.9)	54.8 ± 18.9 (58.4 ± 10.0)†
ψ'	131.5 ± 17.4 (132.7 ± 16.1)	136.9 ± 14.2 (143.1 ± 10.8)‡
ϕ'	185.7 ± 10.9	196.4 ± 21.8 (184.3 ± 10.7)§
ω'	260.6 ± 20.5	255.1 ± 18.0
ω	288.2 ± 12.4	287.4 ± 12.2
ϕ	177.1 ± 12.1	175.4 ± 16.6 (179.0 ± 13.2)¶
χ_{Pur}	59.4 ± 14.4	61.7 ± 14.4
χ_{Pyr}	56.6 ± 15.8	52.2 ± 20.1 (69.4 ± 15.8)‖

Pur, purine; Pyr, pyrimidine.
*Average excluding angles of T_1', which undergoes sugar pucker.
†Average excluding ψ of T_1', which undergoes G-G → G-T transition as well as sugar repuckering.
‡Average excluding ψ' of C_1 and T_1', which undergo sugar repuckering.
§Excluding the ϕ' between T_1' and C_1' and C_1 and G_2, both of which undergo a T → G$^-$ transition.
¶Excluding the ϕ between T_1' and C_1' and C_1 and G_2, both of which have much larger standard deviations than the other angles.
‖Excluding the T_1' and C_1, which undergo sugar repuckering.

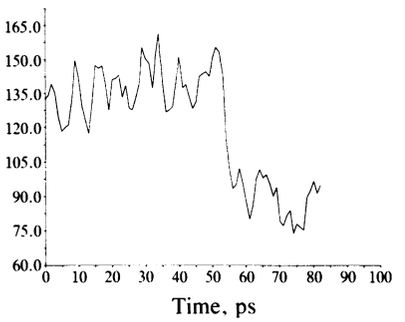

FIG. 1. Value of ψ'(C5′–C4′–C3′–O3′) of T_1' (Thy-13) in simulation with counterions as a function of time.

A more detailed examination of sugar conformation for the simulation with counterions is given in Table 2 using the *q*, *W* notation of Cremer and Pople (14). Both simulations gave results consistent with expectations based on the energy profile for deoxyribose sugars: these are two local minima, C2′ *endo* and C3′ *endo*, with a low barrier (1–2 kcal/mole) between them via O1′ *endo* and a higher barrier (3–4 kcal/mole) over O1′ *exo*/C1′ *endo*. In both simulations, for those sugars that remain near C2′ *endo*, the sugars tend to move toward O1′ *endo* rather than O1′ *exo* conformation. Because of the limited sampling of conformational space in these simulations and the necessity to traverse a barrier to get from C2′ *endo* to C3′ *endo*, we cannot derive a value for the average relative population of C3′ *endo* and C2′ *endo* sugars. The average *q* value in both simulations, 0.35 Å, is reasonably consistent with recent experiments, which suggest that a value nearer 0.35 Å than 0.40 Å fits the solution NMR data better (unpublished data).

It is of interest to examine whether the dihedral angle motions are correlated, as molecular mechanical and prior molecular dynamical simulations suggest that they are. Thus, we have done a systematic analysis of dihedral angle correlations throughout the helix, considering all possible dihedral angle correlations of ψ, ψ', ϕ', ω', ω, ϕ, and χ and report these for the simulation with counterions in Table 3. We divide (Table 3) the correlations into those involving the glycosidic bond, those involving only backbone angles, and "long-range" correlations involving angles separated by more than three bonds.

The correlations involving the glycosidic bond, χ, are quite similar to those found by Levitt (7), although of somewhat smaller magnitude. We found negative correlations with ϕ', ψ, and ω' and positive correlations with ψ' and ϕ.

Table 2. Sugar pucker profiles for simulations with counterions

Base	*q*	% C3′ *endo*	% O1′ *endo*	% C2′ *endo*	% O1′ *exo*	% C1′ *endo*
C_1	0.31 ± 0.08	1.33	24.33	74.21	0.12	0.00
G_2	0.35 ± 0.06	0.00	30.27	69.73	0.00	0.00
C_3	0.35 ± 0.08	0.00	16.10	82.20	1.69	0.00
G_4	0.35 ± 0.05	0.00	12.71	83.41	3.87	0.00
A_5	0.37 ± 0.06	0.00	35.11	64.41	0.48	0.00
T_1'	0.35 ± 0.07	17.19	19.37	63.44	0.00	0.00
C_2'	0.34 ± 0.06	0.00	30.87	66.83	2.30	0.00
G_3'	0.37 ± 0.07	0.00	6.42	93.10	0.48	0.00
C_4'	0.33 ± 0.07	0.00	35.71	61.38	2.91	0.00
G_5'	0.36 ± 0.07	0.00	7.26	91.77	0.97	0.00

C3′ *endo* implies $W = -18$ to 54; O1′ *endo*, $W = 54$ to 126; C2′ *endo*, $W = 126$ to 198; O1′ *exo*, $W = 198$ to 270; C1′ *endo*, $W = 270$ to 342. The notation in this and subsequent tables is to number the bases beginning with the 5′ end and to use primes to denote the bases on the second strand; positions of residues are indicated by subscripts, whereas positions of atoms are on line.

Table 3. Dihedral angle (DA) correlations for simulations with counterions

Correlation coefficients*

r involving χ				*r* involving neighboring DAs			
χ,ψ′	0.42	(0.20 to 0.65)	(0.6)†	ψ,φ′	−0.28	(−0.11 to 0.46)	
χ,φ′	−0.12	(−0.56 to 0.20)	(−0.4)†	φ,ω′	−0.36	(−0.75 to 0.06)	
ψ,χ	−0.27	(−0.53 to −0.01)	(−0.3)†	ω′,ω	−0.16	(−0.47 to 0.37)	
χ,ω′	−0.27	(−0.59 to 0.15)	(−0.4)†	ω,φ	−0.33	(−0.57 to 0.02)	
φ,χ	0.32	(−0.03 to 0.64)	(0.3)†	φ,ψ	−0.22	(−0.53 to −0.01)	
				ψ,ψ′	0.07	(−0.52 to 0.20)	
Large *r* involving DAs separated by more than one angle				**DAs with the most long-range correlations**			
φ′,φ	−0.32	(−0.49 to 0.01)		$C_3\omega'$—3		$G_3'\omega'$—4	
ω′,ψ	−0.49	(−0.16 to −0.73)		$C_3\omega$—3		$C_4'\psi'$—3	
				$T_1'\psi'$—10			
***r* involving DAs separated by one angle**							
ψ′,ω′	−0.35	(−0.77 to 0.28)	(−0.5)†				
φ′,ω	−0.19	(−0.27 to −0.06)					
ω′,φ	−0.07	(−0.34 to 0.37)					
ω,ψ	−0.27	(−0.03 to −0.37)	(−0.4)†				
φ,ψ′	0.37	(0.08 to 0.72)	(0.3)†				
ψ,φ′	0.02	(−0.05 to 0.11)					

*Correlation coefficients (*r*) involving changes in each dihedral angle from its average value throughout the simulation. The value in parentheses next to the average gives the range of coefficients for all angle pairs of this type throughout the structure.
†Correlations found by Levitt (7).

No correlations involving neighboring dihedral angles were noted by Levitt, but we found a number of significant ones, in each case with a negative coefficient. Some of the correlations involving dihedral angles separated by one bond are also significant, and the largest ones found are the same as those noted by Levitt, with ψ′, ω′ and ω, ψ negatively correlated and φ, ψ positively correlated.

A search for dihedral angle correlations involving dihedral angles separated by two, three, and four bonds and correlations involving neighboring ψ′, χ′, and ω′ both intrastrand and across-strand revealed only two that had significant correlations in both simulations, one involving φ′ and φ and the other involving ω′, ψ′. The former angles both terminate at the phosphate, and the latter involves two of the more flexible dihedral angles.

We also analyzed the "long-range" correlations ($r > |0.5|$), and those angles whose motions were "long range" correlated with many others and are listed in Table 3. In the simulation with counterions, there are only five angles with three or more long-range correlations, with the thymine ψ′ (which undergoes a repucker transition) correlating with far more angles than any other. In the simulation without counterions, there are many more long-range correlations and the largest number of these involve the residues (T_1', and C_1; note that residue positions are subscript to differentiate residue designations from on-line atom position designations and that primes denote bases on the second strand) that undergo a sugar puckering transition. In both simulations, ω′ is extensively represented in the "long-range correlation" list.

Table 4. H-bond fluctuations and correlations for simulation with counterions

H bond	Length (min, max)*	Angle (min)†
C_1N4-H···O6G_5'	1.917 ± 0.116 (1.70, 2.36)	158 ± 12 (126)
C_1N3···H-N1G_5'	1.865 ± 0.071 (1.67, 2.10)	165 ± 8 (136)
C_1O2···H-N2G_5'	1.895 ± 0.087 (1.71, 2.22)	162 ± 9 (133)
G_2O6···H-N4C_4'	1.883 ± 0.088 (1.71, 2.25)	162 ± 9 (130)
G_2N1-H···N3C_4'	1.876 ± 0.080 (1.67, 2.27)	164 ± 8 (132)
G_2N2-H···O2C_4'	1.888 ± 0.099 (1.67, 2.21)	161 ± 9 (136)
C_3N4-H···O6G_3'	1.925 ± 0.147 (1.69, 2.71)	160 ± 10 (122)
C_3N3···H-N1G_3'	1.895 ± 0.089 (1.66, 2.15)	162 ± 8 (136)
C_3O2···H-N2G_3'	1.883 ± 0.102 (1.69, 2.27)	157 ± 10 (115)
G_4O6···H-N4C_2'	1.912 ± 0.110 (1.69, 2.28)	161 ± 12 (119)
G_4N1-H···N3C_2'	1.855 ± 0.074 (1.68, 2.09)	167 ± 7 (145)
G_4N2-H···O2C_2'	1.884 ± 0.095 (1.67, 2.37)	163 ± 9 (135)
A_5N6-H···O4T_1'	1.861 ± 0.087 (1.68, 2.26)	165 ± 8 (134)
A_5N1···H-N3T_1'	2.024 ± 0.158 (1.69, 2.69)	157 ± 11 (124)

Correlation coefficients‡

Neighboring H bonds				1–3 H bonds	
1–2	0.33	8–9	0.24	1–3	−0.05
2–3	0.24	10–11	0.23	4–6	−0.07
4–5	0.23	11–12	0.08	7–9	−0.12
5–6	0.22	13–14	0.06	10–12	−0.15
7–8	0.39				

*H-bond length and standard deviations in Å. The minimum and maximum values are given in parentheses.
†H-bond A-H···B angle in degrees, with minimum value in parentheses.
‡Correlation coefficients between selected H bonds.

Table 5. rms deviations of atoms in simulation with counterions

Sugar phosphate backbone		rms distance with counterions*, Å			
		Purines		Pyrimidines	
H	2.08	N9	0.84	N1	0.86 (0.79)†
O5′	1.08 (0.93)†	C8	0.86	C2	0.79 (0.76)†
C5′	1.06 (0.95)†	N7	0.84		
C4′	0.98 (0.89)†	C6	0.75	N3	0.88 (0.80)†
O1′	1.00 (0.93)†	C5	0.77	C4	1.00 (0.88)†
C1′	0.89 (0.84)†	C4	0.76	C5	1.14 (0.96)†
C2′	0.94 (0.85)†	N3	0.79	C6	1.06 (0.91)†
C3′	0.98 (0.86)†	C2	0.75	O2	0.79 (0.81)†
O3′	1.11 (0.96)†	N1	0.76	H3	1.00
P	0.97	O6	0.87	O4	1.58
O_A	1.19	H1	0.77	N4	0.97
O_B	1.19	N2	0.78	N4 H_A	1.10
Na^+	2.65	N2 H_A	0.77	N4 H_B	0.96
		N2 H_B	0.87	C7	2.36
		N6	0.90		
		N6 H_A	0.93		
		N6 H_B	1.10		

*rms distance from the structure at the beginning of simulation (after equilibration for 12 ps).
†Excluding values from terminal A·T base pair.

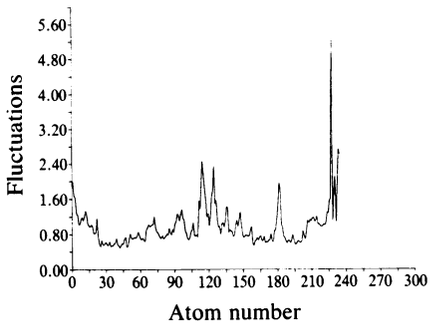

FIG. 2. rms motion of atoms in Å as a function of atom number in simulations with counterions.

In Table 4 we present the distances and angles for the hydrogen bonds and their correlation coefficients for the simulation in which counterions were included. All of the hydrogen bonds are of reasonable average length. There is a correlation between H-bond length and standard deviation, as noted previously by Prabhakaran *et al.* (4, 5); neighboring H-bond lengths are generally positively correlated (7), and the external H-bonds in G·C base pairs are negatively correlated (7), although the correlation coefficients are rather small. The H-bond angles average ≈161–162°, similar to what is found in liquid water, with some rather large exclusions from the "ideal" value of 180°. Similar results were found in the simulation without counterions.

One can also analyze the rms motion of the various atoms around their mean value. Such an analysis is presented in Table 5. Both simulations give a comparable picture: phosphate motions, including the four oxygens to P and C5′, average 1.0–1.2 Å; sugars, 0.9–1.1 Å; and the base atoms, 0.7–0.9 Å. These values are qualitatively similar to those found by Tidor *et al.* (6) and are in the same order as the motions inferred from x-ray temperature factors. Fig. 2 presents the average movement from the 0-ps structure as a function of atom number in the system for the simulation including counterions. One can see some areas of larger movement in such a picture, involving mainly phosphates and counterions.

All of the above indices give one a sense of local motions. What does the DNA helix look like during these simulations? We have calculated a number of the average helical parameters in both simulations (Table 6). Twist gives the average dihedral angle between H-bonded bases, "tilt" gives the average angle each base makes with the helix axis defined by the phosphate atoms, and "helix repeat" gives the relative angle neighboring glycosidic bonds make with each other when projected normal to the helix axis. The twists of the bases are quite similar in the two simulations for the C·G base pairs, although the values are larger for the simulation without counterions. The average twist for the terminal base pairs, particularly the thymine, in the simulations without counterions is very large, as is clear from a visualization of the dynamics trajectory using computer graphics techniques. The base tilts relative to the average helix axis are similar and average ≈10° except for the terminal base C_1 and bases T_1' and C_2', where the tilts are larger. These are also larger in the simulation without counterions than for the simulation with counterions. The helix repeat is the only parameter that differs in a "systematic" way in the two simulations. The simulation with counterions has an average repeat of 10 base pairs per turn, and that without counterions has an average repeat slightly less than 9 base pairs per turn. This result is consistent with the phosphate repulsion forcing the phosphates further apart in the absence of counterions and the structure remaining at a more DNA-like repeat when the phosphates are neutralized.

Table 6. Helix parameters

Base or base pair	With counterions	X-ray*	Without counterions
	Twist†		
C_1·G_5'	22.4 ± 8.6	27.1, 14.8	27.8 ± 12.2
G_2·C_4'	24.2 ± 11.0	22.1, 17.3	29.0 ± 12.4
C_3·C_3'	13.0 ± 7.6	6.3, 6.4	20.5 ± 8.0
G_4·C_2'	14.4 ± 6.6	22.2, 21.6	14.8 ± 8.0
A_5·T_1'	21.6 ± 11.3	24.2, 24.6	41.6 ± 15.7
Average	19.1	20.4, 16.9	26.7
	Tilt‡		
C_1	26.1 ± 11.5	12.6, 37.6	35.6 ± 13.6
G_2	12.1 ± 7.1	6.4, 9.1	9.2 ± 4.4
C_3	11.6 ± 5.6	7.5, 8.5	11.5 ± 5.0
G_4	10.5 ± 5.5	8.9, 10.9	8.4 ± 4.0
A_5	13.1 ± 6.5	16.0, 15.3	11.2 ± 5.9
T_1'	21.1 ± 8.0	9.2, 9.0	26.8 ± 12.1
C_2'	18.5 ± 10.4	12.7, 13.6	25.2 ± 11.0
G_3'	8.7 ± 4.5	1.1, 2.2	11.9 ± 5.2
C_4'	9.1 ± 4.7	20.8, 22.1	11.7 ± 4.7
G_5'	10.8 ± 7.0	4.8, 11.7	12.6 ± 9.5
Average	14.2	10.0, 14.0	16.4
	Helix repeat§		
C_1·G_5'–G_2·C_4'	36.5 ± 4.5	35.0, 36.6	43.4 ± 4.0
G_2·C_4'–C_3·G_3'	34.8 ± 5.7	41.7, 39.3	35.7 ± 2.7
C_3·G_3'–G_4·C_2'	38.8 ± 6.8	28.7, 30.4	42.9 ± 5.2
G_4·C_2'–A_5·T_1'	33.8 ± 4.7	42.3, 38.0	41.1 ± 4.3
Average	36.0	36.9, 36.1	40.8

*Values calculated using the structure reported in ref. 8.
†The angle that the two base pair planes make with each other (in degrees).
‡The angle that bases make with the helix axis defined by the phosphate groups.
§The angle made by the successive N1(N9)–N1(N9) vectors projected onto the helix axis.

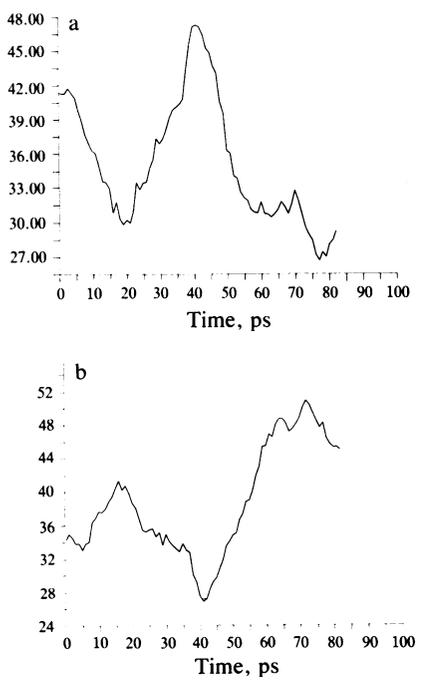

FIG. 3. (*a*) Helix repeat angle (G2·C4′–C3·G3′) plotted as a function of time for the simulation with counterions. (*b*) Same as *a* for angle C3·G3′–G4·C2′.

A comparison with the values of twist and tilt found in the top and bottom base pairs in the crystal structure of d(C-G-C-G-A-A-T-T-C-G-C-G)$_2$ (8) reveals that the average dynamics values are close to that found in the crystal, even though the individual values differ. Most surprising is the fact that in both simulations the central 2-base-pair steps have the opposite difference found in the x-ray values, suggested to be due to Calladine's rules (15, 16), involving steric interactions of the exocyclic base groups in the major and minor grooves of DNA. Such steric effects should be represented in our force field but may be modulated by the electrostatic effects and the rather primitive way long-range electrostatic effects are handled.

Fig. 3 presents the time course of the helix repeat for these central two-base steps and makes clear that they both vary over a wide range during the simulation. Over certain time periods, base step 2 is larger than step 3, so perhaps longer averaging would reverse the trend observed in the average step value. It is also essential to carry out the simulations with longer sequences and with and without explicit solvations to come to more firm conclusions on this point.

In the simulation with counterions, the cations on each chain behave similarly. Beginning with the 5′ end of the DNA, cations 1, 2, and 3 bifurcate between phosphates 1 and 2, 2 and 3, and 3 and 4 and fluctuate near this position throughout much of the simulation. The cation on the 3′ end of each chain begins near phosphate 4. In the case of the first chain, this phosphate remains near this position for much of the simulation, but in the last 10 ps moves to a position in the minor groove equidistant from phosphates on each chain. Cation 4 of the second chain moves toward a position bifurcating phosphates 3 and 4, while cation 3 moves away from cation 4 but still bifurcates the phosphate positions, leaving a charge configuration like $- \ddagger -$; after ≈50 ps, this cation 4 returns to its terminal position near only phosphate 4. Viewing the motions of the cations with computer graphics allows one to visualize their motions and notice the tendency of the cations to avoid each other—namely, one can view this as $- \updownarrow - \ddagger - \updownarrow -$, where the minuses are the phosphate positions and pluses are the cations.

DISCUSSION AND CONCLUSIONS

We have presented a molecular dynamical simulation of double-helical DNA with fully anionic phosphates with and without counterions. Prior models have neglected electrostatics (7) or reduced the charge on the phosphate group (6). Nonetheless, the calculations presented here are primitive because explicit solvation by water has not been included and long-range electrostatic effects have been damped by using a distance-dependent dielectric constant (17) and a nonbonded cutoff of 12 Å.

The simulation of monovalent cations with artificially large radii has shown a good deal of flexibility in counterion positions around DNA. Clementi and Corongiu (18) have studied DNA in the presence of water and (normal size) Na^+ cations using Monte Carlo methods, keeping the DNA fixed. The Na^+ ion fluctuations they report (figure 2 in ref. 18) are significantly smaller than ours (Table 5), but this could be due to the presence of "real" H_2O molecules in their simulation. It is unlikely that either their or our simulations have sufficiently "converged" to definitively deduce counterion structure.

It is interesting to compare the simulations presented here with those of Levitt (7), given the fact that our models (particularly that without counterions) probably exaggerate electrostatic effects and Levitt's model neglects them. Given these differences, as well as the fact that Levitt studied much longer sequences than we did, it is encouraging to note the areas of agreement between the calculations, including average torsional angle values, dihedral angle correlations (although we find more than he), H-bond lengths and fluctuations, and base pair tilts and twists, as well as the qualitative agreement with crystallographic values.

The major differences between the simulations are two. First, we do not find evidence for the periodic large-scale motion noted by Levitt (7), although this may well be due to the fact that our sequence is so short. Second, Levitt's simulations find average helix repeats of ≈11–12.6; our simulations without counterions find 9.0 and with counterions find a repeat nearer 10.0. This is consistent with the neglect of P–P anionic repulsions that allow too small a helix repeat angle, an inclusion of these repulsions without compensating counterions causing a too-large (≈40°) angle and the simulation with counterions giving a reasonable balance.

We emphasize that our long-range goal is to compare the properties and dynamics of normal DNA with mismatched sequence analogs, covalently modified (e.g., thymine dimer or mitomycin cross-linked sequences) and noncovalent (intercalative or nonintercalative) drug–DNA complexes; this goal and our limited computer resources have led us to begin with shorter base sequences than Levitt; a 5-base-pair sequence such as we have chosen is very close to the single-to-double-strand transition point at 298 K. Nonetheless, for such short-time simulations, we expected (and found) the structure to remain B-DNA-like.

Our study presents a detailed analysis of the sugar pucker properties in double-stranded DNA, and the results are in encouraging agreement with NMR experiments (15), with predominantly C2′ *endo* but examples of C3′ *endo* sugar puckers and q values averaging ≈0.35 Å.

We thank W. van Gunsteren for sending us GROMOS, from which we extracted the dynamics code to incorporate into AMBER and which enabled these calculations to be initiated, and M. Levitt for the dynamics display program, which proved invaluable in visualizing the trajectories and for stimulating discussions. We are grateful to the National Institutes of Health (CA-25644) for research support and the University of California, San Francisco, Computer Graphics Lab (supported by RR-1081, R. Langridge, director, and T. Ferrin, system manager) for essential computer graphics displays of structures.

1. Karplus, M. & McCammon, J. (1983) *Annu. Rev. Biochem.* **52,** 263–300.
2. Stillinger, F. & Rahman, A. (1974) *J. Chem. Phys.* **60,** 1545–1557.
3. Rossky, P. & Karplus, M. (1979) *J. Am. Chem. Soc.* **101,** 1913–1937.
4. Prabhakaran, M., Harvey, S., Mao, B. & McCammon, J. (1983) *J. Biomol. Struct. Dyn.* **1,** 357–369.
5. Prabhakaran, M., Harvey, S., Mao, B. & McCammon, J. (1984) *Science* **223,** 1189–1191.
6. Tidor, B., Brooks, B. & Karplus, M. (1983) *J. Biomol. Struct. Dyn.* **1,** 231–252.
7. Levitt, M. (1983) *Cold Spring Harbor Symp. Quant. Biol.* **47,** 251–275.
8. Drew, H., Wing, R., Takano, T., Broka, C., Tanaka, S., Itakura, K. & Dickerson, R. (1981) *Proc. Natl. Acad. Sci. USA* **78,** 2179–2183.
9. Weiner, P. & Kollman, P. (1981) *J. Comp. Chem.* **2,** 287–303.
10. Weiner, S., Kollman, P., Case, D., Singh, U. C., Ghio, C., Alagona, G., Profeta, S. & Weiner, P. (1984) *J. Am. Chem. Soc.* **106,** 765–784.
11. Arnott, S., Campbell-Smith, P. & Chandresekharan, P. (1976) *CRC Handbook of Biochemistry* (CRC, Boca Raton, FL), Vol. 2, pp. 411–422.
12. Berendsen, H. J., Postma, J. P., DiNola, A., van Gunsteren, W. F. & Haak, J. R. (1984) *J. Chem. Phys.*, in press.
13. Kollman, P., Keepers, J. & Weiner, P. (1982) *Biopolymers* **21,** 2345–2376.
14. Cremer, D. & Pople, J. (1975) *J. Am. Chem. Soc.* **97,** 1354–1358.
15. Dickerson, R. (1983) *J. Mol. Biol.* **166,** 419–441.
16. Calladine, C. (1982) *J. Mol. Biol.* **161,** 343–352.
17. Blaney, J., Weiner, P., Dearing, A., Kollman, P. A., Jorgensen, E. C., Oatley, S., Burridge, J. & Blake, C. (1982) *J. Am. Chem. Soc.* **104,** 6424–6434.
18. Clementi, E. & Corongiu, G. (1982) *Biopolymers* **21,** 763–777.